Atomic Quadrupole Moment Measurement Using Dynamic Decoupling

R. Shaniv, N. Akerman, and R. Ozeri
Department of Physics of Complex Systems, Weizmann Institute of Science, Rehovot 7610001, Israel
(Received 25 November 2015; published 8 April 2016)

We present a method that uses dynamic decoupling of a multilevel quantum probe to distinguish small frequency shifts that depend on m_j^2, where m_j^2 is the angular momentum of level $|j\rangle$ along the quantization axis, from large noisy shifts that are linear in m_j, such as those due to magnetic field noise. Using this method we measured the electric-quadrupole moment of the $4D_{5/2}$ level in $^{88}Sr^+$ to be $2.973^{+0.026}_{-0.033} ea_0^2$. Our measurement improves the uncertainty of this value by an order of magnitude and thus helps mitigate an important systematic uncertainty in $^{88}Sr^+$ based optical atomic clocks and verifies complicated many-body quantum calculations.

DOI: 10.1103/PhysRevLett.116.140801

Increasing the coherence time of quantum superpositions is an ongoing research topic. From the quantum information point of view, prolonging the coherence time allows for the performance of a larger number of coherent operations, making more complex quantum computation algorithms possible [1] as well as longer-living quantum memory [2]. From a metrology perspective, decoherence poses a time limit on the coherent evolution of a quantum probe when used to measure some physical quantity, thereby limiting the accuracy with which this quantity is evaluated.

Several methods were developed and demonstrated to increase the coherence time of quantum systems. Examples include decoherence-free subspaces (DFSs) [3,4], quantum error correction codes (QECCs) [5,6] and dynamic decoupling (DD) methods [7,8]. DD methods are used for correcting errors in various physical systems, ranging from NMR, where these methods appeared for the first time [9], to atomic, solid-state, and photonic qubits [10–13]. The implementation of DD methods is simple relative to DFSs and QECCs as it does not require the entanglement of multiqubit arrays and can rely solely on single qubit operations. All of the decoherence suppression methods above have been suggested or used to improve quantum metrology as well. In the context of metrology, a method is chosen such that on top of noise suppression the measured signal is coherently accumulated. Specifically, DD has been successfully used in solid-state and atomic probes for precision magnetometry [14–17] light shifts [18] and force detection [19].

In this Letter we present a new DD method which decouples a superposition of atomic levels in a single trapped $^{88}Sr^+$ ion from external magnetic field noise while measuring the electric-quadrupole shift induced by an electric field gradient. In contrast with the usual two-level quantum probes, here we take advantage of the sixfold $4D_{5/2}$ Zeeman manifold of equidistant levels. Using this method, we measured the quadrupole moment of the $4D_{5/2}$ level in $^{88}Sr^+$ to be $2.973^{+0.026}_{-0.033} ea_0^2$, where e is the electron charge and a_0 is the Bohr radius.

The quadrupole moment of an atomic state is a measure of its deviation from perfect spherical symmetry. While ground state S orbitals are spherically symmetric, higher levels, such as states in the D manifold have a finite electric-quadrupole moment. This electric-quadrupole moment couples to an electric field gradient across the atomic wave function. The resulting energy shift is usually small in comparison to other shifts, e.g., the Zeeman shift, due to the small atomic length scale over which the electric field has to change. However small, this is nevertheless an important systematic shift in ion-trap optical atomic clocks [20]. Here, electric field gradients are inherent to the trap and induce typical fractional shifts to optical electric-quadrupole clock transitions on the order of 10^{-13}. Evaluating the above shift requires reliable knowledge of the quadrupole moment of the levels involved.

We performed our measurement on a single $^{88}Sr^+$ ion trapped in a linear Paul trap. The $S_{1/2} \rightarrow D_{5/2}$ electric-quadrupole optical transition of this ion is investigated as a possible atomic time standard in several experiments [21,22]. The quadrupole moment of the $4D_{5/2}$ level in $^{88}Sr^+$ was previously measured [23]. Measurements of the D level quadrupole moment of $^{199}Hg^+$ [24] and $^{171}Yb^+$ [25] were also published. In addition, a method for measuring the quadrupole moment of $^{40}Ca^+$ using an entangled superposition of two ions was experimentally demonstrated [26]. Our new method yields a measured value for the quadrupole moment in the $4D_{5/2}$ level in a $^{88}Sr^+$ ion with about ten times smaller uncertainty in comparison to the previous measurement, and it requires a single ion only.

The relevant levels for our experiment are the twofold $5S_{1/2}$ ground level $|S, m_j\rangle$, and the sixfold $4D_{5/2}$ level $|D, m_j\rangle$ shown schematically in Fig. 1. A constant magnetic field of, typically, $B = 3 \times 10^{-4}$ T, splits the different Zeeman states in both levels. This magnetic field is generated by three Helmholtz coils in three orthogonal axes. The Zeeman frequency splitting between two

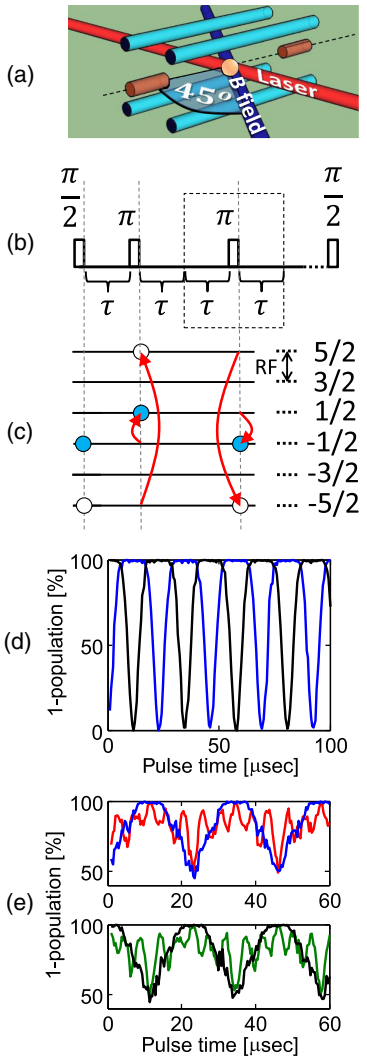

FIG. 1. Layout of the experiment and the pulse sequence scheme. (a) Scheme of the trap structure and orientation with respect to the laser $\vec{k}$ vector and the magnetic field directions. The trap axis is shown by the dashed line passing through both end caps. The laser direction is at a right angle with respect to the trap axis, and the magnetic field direction can be scanned and is shown here to be at a 45° angle with respect to both the laser and the trap axis. (b) Pulse sequence for the measurement of the quadrupole shift. The dashed frame marks the sequence building block which is being repeated. (c) The definition of a rf π pulse. The blue and white circles mark the two amplitudes, and the numbers in the right-hand column denote the different m_J values. The black two-sided arrow marks the rf frequency used to drive the transition. (d),(e) Rabi oscillations on the sixfold $4D_{5/2}$ energy level for initial states $|\psi_i\rangle = |D,-\frac{5}{2}\rangle$ and $|\psi_i\rangle = \frac{1}{\sqrt{2}}(|D,-\frac{5}{2}\rangle + |D,-\frac{1}{2}\rangle)$, respectively. The vertical axis shows the population outside the detected sublevel. Blue, red, green, and black lines correspond to the population in the levels $m_J = -\frac{5}{2}$, $m_J = -\frac{1}{2}$, $m_J = \frac{1}{2}$, and $m_J = \frac{5}{2}$, respectively. Both the upper and lower plots in (e) correspond to the same experiment, separated for clarity.

adjacent levels in the $4D_{5/2}$ manifold Δf_Z is typically around 5 MHz. The ion $5S_{1/2} \rightarrow 4D_{5/2}$ transition is addressed with a 674 nm narrow linewidth laser, with spectral fast linewidth of 100 Hz over several minutes [27]. Spin rotations are generated by radio frequency (rf) fields at the Zeeman splitting frequency. The orientation of the trap electrodes, the laser k vector, and the quantization magnetic field are shown in Fig. 1(a). Ion state detection is performed using state selective fluorescence on a strong dipole allowed transition at 422 nm [28]. More details about the experimental apparatus can be found in Ref. [29].

The electric dc potential generated by these electrodes is well approximated by

$$U = \frac{1}{4}\frac{dE_z}{dz}(x^2 + y^2 - 2z^2), \tag{1}$$

where z is the direction of the trap axis, and the resulting shift of state $|D, m_j\rangle$ level is given by [30]

$$\Delta\nu_Q = \frac{1}{4h}\frac{dE_z}{dz}\Theta\left(D,\frac{5}{2}\right)\frac{35 - 12m_j^2}{40}[3\cos^2(\beta) - 1]. \tag{2}$$

Here, (dE_z/dz) is the electric field gradient along the quadrupole axis, $\Theta(D,\frac{5}{2})$ is the $4D_{5/2}$ level quadrupole moment and β is the angle between the quantization axis set by the magnetic field and the quadrupole axis set by the trap geometry. In our trap this shift is on the order of 50 Hz resulting from typical $(dE_z/dz) \sim 100(V/mm^2)$. This small shift is usually overshadowed by the much larger time variation in Zeeman shifts, typically on the order of a few kilohertz in several milliseconds. In order to measure the quadrupole shift, we developed a DD sequence that employs the equidistant $4D_{5/2}$ Zeeman sublevels to decouple our ion from effects linear with m_J, while leaving it susceptible to shifts that depend on m_J^2.

Our experimental sequence is shown in Fig. 1(b). We begin the sequence by optically pumping the ion to the $|S,-\frac{1}{2}\rangle$ state. We then apply a $(\pi/2)$ pulse on the $|S,-\frac{1}{2}\rangle \rightarrow |D,-\frac{5}{2}\rangle$ transition, followed by a π pulse on the $|S,-\frac{1}{2}\rangle \rightarrow |D,-\frac{1}{2}\rangle$ transition using the 674 nm laser. These two pulses serve as the first $(\pi/2)$ pulse in a generalized Ramsey experiment, initializing the state $|\psi_i\rangle = \frac{1}{\sqrt{2}}(|D,-\frac{5}{2}\rangle + |D,-\frac{1}{2}\rangle)$. After preparing this initial state, a sequence of rf spin-echo pulses is repeated multiple times. Each spin-echo pulse is preceded and followed by a wait time τ; see Fig. 4(b). The rf echo pulses are resonant with the Zeeman splitting of levels in the $D_{5/2}$, $f_{\mathrm{rf}} = \Delta f_Z$, leading to precession of the spin $\frac{5}{2}$ in this manifold. The operation of this rf pulse is shown in Fig. 1(c), and examples of this Rabi nutation under this large spin rotation are shown in Figs. 1(d) and 1(e). The rf pulse maps our ion from the $\{|D,-\frac{5}{2}\rangle, |D,-\frac{1}{2}\rangle\}$ subspace to the $\{|D,\frac{5}{2}\rangle, |D,\frac{1}{2}\rangle\}$ subspace and vice versa. Since the separation of the levels in

each of these subspaces due to the magnetic field is the same in magnitude and opposite in sign, the superposition phases accumulated in the wait times before and after each echo pulse due to a constant magnetic field cancel each other. Therefore, the superposition phase does not depend on the magnetic field to the first order. According to Eq. (1), the quadrupole shift depends on m_J^2, and therefore its contribution to the superposition phase has the same sign in the two subspaces and hence is added rather than canceled. The phase accumulated during each wait time τ is given by the difference between the quadrupole shift of the $m = \frac{5}{2}$ and $m = \frac{1}{2}$ states,

$$\Delta\phi_{\mathrm{arm}} = \frac{9}{20\hbar}\frac{dE_z}{dz}\Theta\left(D, \frac{5}{2}\right)[3\cos^2(\beta) - 1]\tau. \qquad (3)$$

Echo pulses with two wait times are repeated an even number of times, where the phase of the different rf pulses alternates between 0 and π, to correct for pulse area imperfections. After the last τ wait time, the ion is in a superposition $|\psi_f\rangle = \frac{1}{\sqrt{2}}(|D, -\frac{5}{2}\rangle + e^{i\phi_{\mathrm{total}}}|D, -\frac{1}{2}\rangle)$, where ϕ_{total} is the final superposition phase, and is equal to $\phi_{\mathrm{total}} = 2n\Delta\phi_{\mathrm{arm}}$, where n is the number of rf pulses.

In order to detect this phase, we transfer the $|D, -\frac{5}{2}\rangle$ state to the $|S, -\frac{1}{2}\rangle$ state, mapping $|\psi_f\rangle$ into $|\psi_{\mathrm{det}}\rangle = \frac{1}{\sqrt{2}}(|S, -\frac{1}{2}\rangle + e^{i\phi_{\mathrm{total}}}|D, -\frac{1}{2}\rangle)$. We measure ϕ_{total} by completing a Ramsey sequence and applying a $(\pi/2)$ pulse on the $|S, -\frac{1}{2}\rangle \rightarrow |D, -\frac{1}{2}\rangle$ transition with laser phase ϕ_{laser} with respect to the immediately preceding laser pulse, followed by state-selective fluorescence at 422 nm. Note that the laser phase should be stable only between the two last detection pulses and the two initialization pulses, but it does not play any role during the quadrupole phase accumulation time. Therefore, many systematic effects that affected previous quadrupole shift measurements [23–25] such as ac Stark shifts, second-order Doppler effects, and their dependence on micromotion, as well as limitations imposed by the clock transition laser phase noise, are irrelevant. The probability of measuring the ion in the D level vs the ϕ_{laser} is shown in the inset of the top panel of Fig. 2. The accumulated phase ϕ_{total} is estimated by a maximum likelihood fit. In order to reject the phase accumulated during the pulses in the sequence (smaller than 0.1 rad), we subtract the phase measured in a reference experiment with $\tau = 0$.

To measure the quadrupole moment, $\Theta(D, \frac{5}{2})$, one has to determine both (dE_z/dz) and β. The electric field gradient was estimated by measuring the ion harmonic frequency in the trap using resonant excitation. The gradient in the electric field is then given by $(dE_z/dz) = (m\omega^2/q)$, where m, ω, and q are the mass of the ion, the trap frequency in the quadrupole axis, and the charge of the ion, respectively. The contribution of the rf trap electric fields to the axial trap frequency was measured and subtracted from the electric

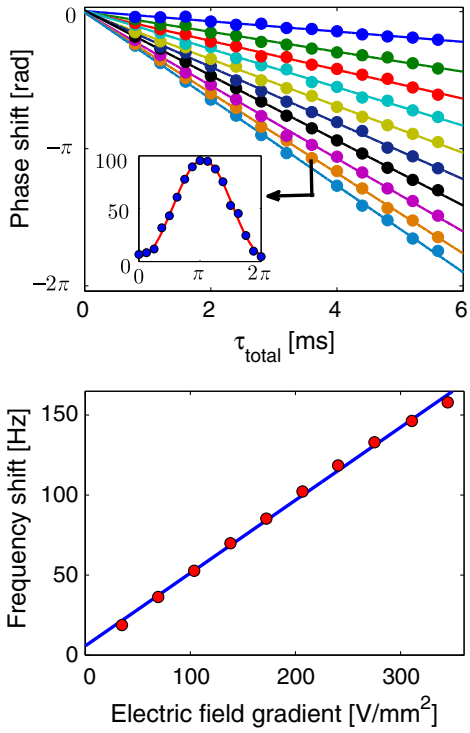

FIG. 2. Measured phase and frequency shifts as a function of the total experiment time τ_{total} and (dE_z/dz). (Top panel) Ramsey phase measurement as a function of the total experiment time, for different electric field gradients shown in different colors. Filled circles represent the phase of a Ramsey fringe fit. Solid lines show fitted linear curves to the data. As seen, the phase increases linearly with time. A typical Ramsey fringe is shown in the inset. (Bottom panel) Quadrupole frequency shift as a function of the electric field gradient. Each point corresponds to the absolute value of a slope (in hertz) of each line in (a). 95% confidence error bars for one of the points are shown in the inset. The frequency shift is linear in the applied gradient within the measurement uncertainty. A solid line shows a fitted linear slope to the data.

gradient estimation. The error in the electric field gradient estimation (0.1%) is significantly small compared to our statistical uncertainty.

The top panel in Fig. 2 shows the measured ϕ_{total} as a function of τ_{total} for various electric field gradients. In all of these measurements, the magnetic field was aligned roughly at 45° with respect to the quadrupole axis ($\beta \approx \pi/4$). Indeed the acquired phase varies linearly with τ_{total}. The frequency shift was estimated by a maximum likelihood linear fit and is shown vs the electric field gradient in the top panel in Fig. 2. As seen, the frequency shift we measure is linear in the applied electric field gradient within our measurement error.

Instead of determining β precisely, we measured the phase shift for different magnetic field directions. The magnetic field direction was varied by changing the relative current between the three Helmholtz coils. The main Helmholtz coil was held at a constant current, while the current in a perpendicular coil was varied [31]. We used the

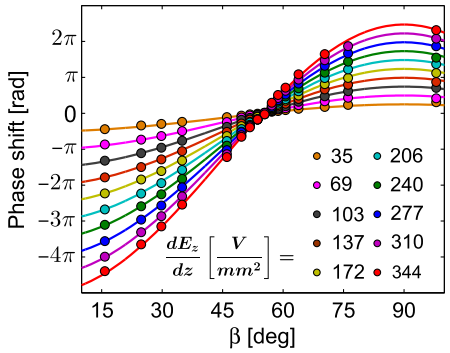

FIG. 3. The total accumulated phase due to the quadrupole shift, ϕ_{total}, as a function of the magnetic field angle with respect to the quadrupole axis, β, for different values of (dE_z/dz). The total phase accumulation time for all points was $\tau_{\text{total}} = 4$ msec. Filled circles are measured phases. For each angle, the phase shift was linearly fitted and the phase offset for $(dE_z/dz) = 0$ (always below 0.2 rad) was subtracted from the data set. The error bars are too small to be seen on this scale. Solid lines are generated by a maximum likelihood fit to Eq. (3), taking the entire data set into account.

magnetic field sensitive transition $|S,-\frac{1}{2}\rangle \rightarrow |S,\frac{1}{2}\rangle$ to measure the magnetic field magnitude on the ion, and therefore also the angle of the magnetic field relative to the base angle defined by the main coil direction, β_0. The measured superposition phase as a function of β is shown in Fig. 3. For each β the superposition phase is seen to be linear with (dE_z/dz). A linear fit reveals a small phase offset (always below 0.2 rad in magnitude) when $(dE_z/dz) = 0$, which is removed independently for each β. Since both (dE_z/dz) and τ are precisely known, we used a maximum likelihood fit to estimate both β_0 and $\Theta(D, 5/2)$.

The measurement result for the quadrupole moment could be affected by several systematic effects. Since a second-order Zeeman shift depends on m_j^2, it is not canceled by our sequence. The second-order Zeeman shift in our experiment is estimated to be less than 0.5 Hz and below our measurement accuracy. In addition, as was mentioned above, phase offsets extrapolated at zero electric field gradient were subtracted from the data, leaving only phases which depend on the electric field gradient to be accounted for. Other types of systematic errors could arise from trap imperfections. Equation (1) relies on the trap dc potential having perfect cylindrical symmetry, but the more general way of writing the potential that still satisfies the Laplace equation is $U = \frac{1}{4}(dE_z/dz)[(x^2 + y^2 - 2z^2) + \epsilon(x^2 - y^2)]$. Here, we take into account a possible dc nondegeneracy in the radial frequencies (ϵ). This term yields a phase proportional to $\sin^2(\beta)$ which is small since it reflects the deviation of the magnetic field direction from the plane defined by the trap axis and the direction $\vec{x} + \vec{y}$, where $\vec{x}, \vec{y}$ are vectors parallel to the trap x, y axes. We take this term into account by adding it to the maximum likelihood fit for the final quadrupole moment value. An additional systematic error could have resulted from fields, e.g., a magnetic field, that oscillate synchronously with our DD sequence. Such fields are highly unlikely, as our sequence is not synchronized with any external trigger.

TABLE I. A comparison between different measurements and calculations of the $4D_{5/2}$ level quadrupole moment in $^{88}Sr^+$.

This work		Previous measurement
$2.973^{+0.026}_{-0.033}$		2.6 ± 0.3[a]
Theoretical calculations		
3.048[b]	2.94 ± 0.07[c]	2.935 ± 0.017[d]

[a]Reference [23].
[b]Reference [32].
[c]Reference [33].
[d]Reference [34].

The final result and its statistical 95% confidence interval are $\Theta(D, \frac{5}{2}) = 2.973^{+0.026}_{-0.033} e a_0^2$. Our statistical error is consistent with quantum projection noise. All of the systematic uncertainties mentioned above are negligible compared to the statistical uncertainty. Our result as well as the results of previous measurements and calculations is summarized in Table I. Our measurement is in good agreement with the theoretical calculations and is 1.2σ away from the previous measurement, with an uncertainty an order of magnitude smaller.

To conclude, we developed a new method that combines dynamic decoupling with the use of a multiequidistant-level quantum probe to distinguish a small frequency shift that depends on m_j^2 from large noisy shifts that depend linearly on m_j. We thus measured the quadrupole shift of the $4D_{5/2}$ level in $^{88}Sr^+$ while decoupling it from magnetic field noise. Our method allowed us to measure the quadrupole moment of the $4D_{5/2}$ level with 1.1% uncertainty. Our measurement verifies complicated many-body quantum calculations of atomic structure. In the future, this method could be used to measure second-order Zeeman shifts as well. Since our method only requires a single ion and no entanglement, it can easily be used in order to place bounds on possible systematic shifts in precision optical spectroscopy.

We thank Tom Manovitz for the many helpful discussions. This work was supported by the Crown Photonics Center, ICore—Israeli Excellence Center Circle of Light, the Israeli Science Foundation, the Israeli Ministry of Science Technology and Space, and the European Research Council (Consolidator Grant No. 616919-Ionology).

[1] D. P. DiVincenzo, Quantum computation, Science **270**, 255 (1995).
[2] C. Langer, R. Ozeri, J. D. Jost, J. Chiaverini, B. DeMarco, A. Ben-Kish, R. B. Blakestad, J. Britton, D. B. Hume, W. M. Itano *et al.*, Long-Lived Qubit Memory Using Atomic Ions, Phys. Rev. Lett. **95**, 060502 (2005).

[3] D. A. Lidar, Review of decoherence free subspaces, noiseless subsystems, and dynamical decoupling, Adv. Chem. Phys. **154**, 295 (2014).
[4] D. Kielpinski, V. Meyer, M. A. Rowe, C. A. Sackett, W. M. Itano, C. Monroe, and D. J. Wineland, A decoherence-free quantum memory using trapped ions, Science **291**, 1013 (2001).
[5] Peter W. Shor, Scheme for reducing decoherence in quantum computer memory, Phys. Rev. A **52**, R2493 (1995).
[6] A. M. Steane, Error Correcting Codes in Quantum Theory, Phys. Rev. Lett. **77**, 793 (1996).
[7] L. Viola and S. Lloyd, Dynamical suppression of decoherence in two-state quantum systems, Phys. Rev. A **58**, 2733 (1998).
[8] G. Gordon, N. Erez, and G. Kurizki, Universal dynamical decoherence control of noisy single-and multi-qubit systems, J. Phys. B **40**, S75 (2007).
[9] E. L. Hahn, Spin echoes, Phys. Rev. **80**, 580 (1950).
[10] S. E. Beavan, E. Fraval, M. J. Sellars, and J. J. Longdell, Demonstration of the reduction of decoherent errors in a solid-state qubit using dynamic decoupling techniques, Phys. Rev. A **80**, 032308 (2009).
[11] S. Damodarakurup, M. Lucamarini, G. Di Giuseppe, D. Vitali, and P. Tombesi, Experimental Inhibition of Decoherence on Flying Qubits via "Bang-Bang" Control, Phys. Rev. Lett. **103**, 040502 (2009).
[12] Y. Sagi, I. Almog, and N. Davidson, Suppression of collisional decoherence in optically trapped atomic ensemble by bang-bang dynamical decoupling, in *Proceedings of the Quantum Electronics and Laser Science Conference, San Jose, 2010* (Optical Society of America, Washington, DC, 2010), p. QThJ1.
[13] M. Lucamarini, G. Di Giuseppe, S. Damodarakurup, D. Vitali, and P. Tombesi, Suppression of polarization decoherence for traveling light pulses via bang-bang dynamical decoupling, Phys. Rev. A **83**, 032320 (2011).
[14] L. T. Hall, C. D. Hill, J. H. Cole, and L. C. L. Hollenberg, Ultrasensitive diamond magnetometry using optimal dynamic decoupling, Phys. Rev. B **82**, 045208 (2010).
[15] V. V. Dobrovitski, G. de Lange, D. Ristè, and R. Hanson, Single-Spin Magnetometry with Multipulse Sensing Sequences, Phys. Rev. Lett. **106**, 080802 (2011).
[16] S. Kotler, N. Akerman, Y. Glickman, and R. Ozeri, Nonlinear Single-Spin Spectrum Analyzer, Phys. Rev. Lett. **110**, 110503 (2013).
[17] I. Baumgart, J.-M. Cai, A. Retzker, M. B. Plenio, and Ch. Wunderlich, Ultrasensitive magnetometer using a single atom, arXiv:1411.7893.
[18] S. Kotler, N. Akerman, Y. Glickman, A. Keselman, and R. Ozeri, Single-ion quantum lock-in amplifier, Nature (London) **473**, 61 (2011).
[19] R. Shaniv, and R. Ozeri, Quantum lock-in force sensing using optical clock doppler velocimetry, arXiv:1602.08645
[20] N. Poli, C. W. Oates, P. Gill, and G. M. Tino, Optical atomic clocks, Riv. Nuovo Cimento Soc. Ital. Fis. **036**, 555 (2013).
[21] H. S. Margolis, G. P. Barwood, G. Huang, H. A. Klein, S. N. Lea, K. Szymaniec, and P. Gill, Hertz-level measurement of the optical clock frequency in a single $^{88}Sr^{+}$ ion, Science **306**, 1355 (2004).
[22] P. Dubé, A. A. Madej, Z. Zhou, and J. E. Bernard, Evaluation of systematic shifts of the $^{88}Sr^{+}$ single-ion optical frequency standard at the 10–17 level, Phys. Rev. A **87**, 023806 (2013).
[23] G. P. Barwood, H. S. Margolis, G. Huang, P. Gill, and H. A. Klein, Measurement of the Electric Quadrupole Moment of the $4d^2D_{5/2}$ Level in $^{88}Sr^{+}$, Phys. Rev. Lett. **93**, 133001 (2004).
[24] W. H. Oskay, W. M. Itano, and J. C. Bergquist, Measurement of the $^{199}Hg^{+}$ $5d^96s^{22}D_{5/2}$ Electric Quadrupole Moment and a Constraint on the Quadrupole Shift, Phys. Rev. Lett. **94**, 163001 (2005).
[25] T. Schneider, E. Peik, and Chr. Tamm, Sub-Hertz Optical Frequency Comparisons between Two Trapped $^{171}Yb^{+}$ Ions, Phys. Rev. Lett. **94**, 230801 (2005).
[26] C. F. Roos, M. Chwalla, K. Kim, M. Riebe, and R. Blatt, 'Designer atoms' for quantum metrology., Nature (London) **443**, 316 (2006).
[27] N. Akerman, N. Navon, S. Kotler, Y. Glickman, and R. Ozeri, Universal gate-set for trapped-ion qubits using a narrow linewidth diode laser, New J. Phys. **17**, 113060 (2015).
[28] A. Keselman, Y. Glickman, N. Akerman, S. Kotler, and R. Ozeri, High-fidelity state detection and tomography of a single-ion Zeeman qubit, New J. Phys. **13**, 073027 (2011).
[29] N. Akerman, Y. Glickman, S. Kotler, A. Keselman, and R. Ozeri, Quantum control of $^{88}Sr^{+}$ in a miniature linear Paul trap, Appl. Phys. B **107**, 1167 (2012).
[30] W. M. Itano, External-field shifts of the $^{199}Hg^{+}$ optical frequency standard, J. Res. Natl. Inst. Stand. Technol..
[31] Magnetic field components orthogonal to the table were compensated for. The magnetic field direction was parallel to the table to within 3 deg of uncertainty.
[32] W. M. Itano, Quadrupole moments and hyperfine constants of metastable states of Ca^{+}, Sr^{+}, Ba_{+}, Yb_{+}, Hg_{+}, and Au, Phys. Rev. A **73**, 022510 (2006).
[33] C. Sur, K. V. P. Latha, B. K. Sahoo, R. K. Chaudhuri, B. P. Das, and D. Mukherjee, Electric Quadrupole Moments of the *d* States of Alkaline-Earth-Metal Ions, Phys. Rev. Lett. **96**, 193001 (2006).
[34] D. Jiang, B. Arora, and M. S. Safronova, Electric quadrupole moments of metastable states of Ca^{+}, Sr^{+}, and Ba^{+}, Phys. Rev. A **78**, 022514 (2008).